Solvation of triplet Rydberg states of molecular hydrogen in superfluid helium

Toni Kiljunen,* Lauri Lehtovaara, Henrik Kunttu, and Jussi Eloranta†
Department of Chemistry, University of Jyväskylä, P. O. Box 35, FIN-40014, Jyväskylä, Finland
(Received 25 September 2003; published 26 January 2004)

We report *ab initio* interaction potentials, transition dipole moments, and radiative lifetimes for the four lowest triplet states of H_2: $b\ ^3\Sigma_u^+$, $c\ ^3\Pi_u$, $a\ ^3\Sigma_g^+$, and $e\ ^3\Sigma_u^+$, and their response to the perturbation due to approaching ground state He atom. Hybrid density functional–quantum Monte Carlo calculations employing the *ab initio* interaction potentials are then used for calculating the liquid structure around the molecular excimers in bulk superfluid ^{4}He. Calculations demonstrate a wide variety of possible solvation structures, both spherical and highly anisotropic in geometry, depending on the electronic state of H_2. The experimentally observed H_2 ($^3e \rightarrow {}^3a$) emission bands [Trottier *et al.*, Phys. Rev. A **61**, 052504 (2000)] are simulated and the origins of the line shifts discussed. Absorption spectra of the same system are predicted to be broader and more blue shifted compared to the gas phase. Feasibility of the metastable ^3c state for absorption experiments in liquid helium is proposed.

DOI: 10.1103/PhysRevA.69.012506 PACS number(s): 33.20.Kf, 33.70.Jg, 31.15.Ar

I. INTRODUCTION

Solvation of molecular impurities in superfluid helium has been a subject of intensive experimental and theoretical studies. Mainly two experimental approaches have been attempted to solvate molecular species in the superfluid: embedding impurities in helium droplets [1] and injecting impurities directly into bulk superfluid helium [2]. The helium droplet approach has been most successful whereas only very few bulk helium experiments have been reported (O_2, N_2, He_2, H_2, metal dimers and trimers) [3,4,5,6,7,8]. Even though the helium droplet experiments [1] indicate that many molecules are sufficiently soluble in liquid helium for spectroscopic studies, the bulk experiments appear to suffer from low concentration of molecules [2,9]. Despite the success of the helium droplet experiments, there are some limitations in its applicability as only reduced sample pressure and temperature regions in the phase diagram can be accessed. Furthermore, the finite droplet size may induce unwanted boundary effects, which can complicate theoretical analysis and limit its applicability in the dynamic studies of the superfluid. For these reasons it is desirable to develop experimental approach for injecting molecular species in superfluid bulk helium.

A serious problem in the bulk helium experiments is diffusion mediated clustering of molecules. In fact, the molecular oxygen and nitrogen emissions have been assigned to originate from clusters rather than well-isolated species [3]. As such these do not represent pure molecular solvation in bulk helium. In this respect only three clear examples remain: He_2*, H_2* and the metal clusters. The first two cases have been observed in their metastable triplet electronic states. The intrinsic He_2* excimers were generated by bombarding the liquid by highly energetic particles [4] or by using strong laser field ionization [10]. In these experiments both absorption and emission spectra were recorded as a function of sample pressure and temperature. Analysis of the spectral line shifts and line broadening yielded detailed information on the solvent structure around the molecule [11]. In general, it has been observed that the absorption spectra experience greater perturbation than emission spectra due to stronger electronic coupling to the surrounding liquid. In addition to static solvation, recent time resolved experiments have provided information on dynamic properties of superfluid helium as well as its viscous response on molecular scales [12,13]. In the case of metal clusters, laser ablation of metal target embedded in the superfluid was used in generating a metal atom flow into the liquid. Subsequent atom diffusion and recombination resulted in formation of metal dimers and trimers. Both optical absorption and emission studies of such species were performed [8]. A similar idea was used for H_2* excimer, where a solid molecular hydrogen target was embedded into liquid helium and irradiated by a proton beam [7]. This produced excited triplet state H_2* molecules which were ejected into the surrounding liquid helium held at 4.2 K. The molecular Rydberg state emissions were monitored in the infrared whereas no absorption studies were made. The emission lines were slightly broadened and shifted as compared to their gas phase values. Such changes in lineshapes originate from the excimer-liquid coupling.

In order to aid the experimental efforts it is important to understand the microscopic mechanism of molecular solvation and solvation dynamics in superfluid helium. For time independent description, mainly three classes of theoretical methods have been applied: classical bubble model [14], density functional theory (DFT) [15,16,17,18], and quantum Monte Carlo (QMC) [19]. The bubble model typically includes four terms, which describe the quantum kinetic energy of the vacuum-gas-liquid interface, bubble surface tension, pressure-volume work, and impurity-liquid potential. This energy expression contains a mixture of quantum and classical terms, which, in turn, contain a number of adjustable parameters. Often these parameters have been varied in

*Present address: Institut für Experimentalphysik, Freie Universität Berlin, Arnimallee 14, 14195 Berlin, Germany.
†Corresponding author. Electronic address: eloranta@jyu.fi

such a way that agreement with experimental data is achieved. Furthermore, such calculations assume a specific form for the density function representing the helium liquid-gas interface. This model will, in many cases, give correct qualitative picture of the impurity solvation provided that the liquid is distributed spherically around the impurity. For small angular distortions modified density trial functions have been developed [20].

The DFT is also an approximate method but it has been more thoroughly calibrated against the known properties of superfluid helium. The key differences to the bubble model are: the method of calibration, the total energy expression does not rely on classical terms like surface tension, and it is possible to properly formulate the Euler-Lagrange–type equations from the energy functional. The latter property is essential, for example, when the impurity-He potential is sufficiently bound (''snowball'' structures), anisotropic (nonspherical ''bubbles''), or it causes strong density modulations in the liquid. Simple trial density functions would obviously fail in such cases. The DFT method has been previously applied for describing the He_2* excimer in superfluid helium both in its time dependent and time independent forms [11,13].

Finally, we note that the most exact approaches rely on the QMC where particle-particle interactions are described exactly and the only uncertainty arises from statistical sampling of the high dimensional wave function. From the practical point of view the QMC calculations of bulk liquid are computationally more demanding than the corresponding DFT calculations, and have only very limited use in describing superfluid dynamics. Especially in the strongly bound regimes, however, the QMC methods are expected to be more reliable than DFT because the known functionals have not been calibrated to properly deal with highly inhomogeneous liquid densities.

All the described methods require impurity-liquid helium potential as input. For some Rydberg state impurities the electron densities can be obtained using approximate single electron methods. Essentially, these calculations treat the excimer as an one electron ''atom'' with an effective screened core charge [6]. Once the Rydberg electron wave function is known, the excimer-impurity potential can then be calculated by convoluting the electron-helium pseudopotential with the Rydberg electron density [13,21]. Again, such an approach has a number of adjustable parameters, which in combination with the bubble model parameters, should allow the model to fit almost any data. For this reason it is essential to combine high level *ab initio* calculations [22] with the most advanced QMC and DFT methods [17,18] in order to obtain unbiased theoretical description of the impurity solvation process.

In this work we concentrate on static solvation of the triplet state H_2* excimer impurity in superfluid helium by first calculating the helium-H_2* pair interactions using accurate *ab initio* methods. Then we proceed to calculate the liquid ^{4}He solvation structures around the H_2* excimer using both DFT and hybrid DFT/QMC methods. The numerical calculations are carried out in 1D for spherically symmetric cases as well as in full 3D for nonspherical ones. Finally, we concentrate on spectral shifts and shapes of absorption and emission spectra and suggest new experimental procedures for obtaining more information on the present system.

II. COMPUTATIONAL DETAILS

The present *ab initio* computational approach is similar to that described in Refs. [11,22], where solvation of the triplet He_2* Rydberg excimers in superfluid helium was studied. In this paper we concentrate on molecular hydrogen with states $b\ ^3\Sigma_u^+\ (1s\sigma_g\,1s\sigma_u)$, $c\ ^3\Pi_u\ (1s\sigma_g\,2p\pi_u)$, $a\ ^3\Sigma_g^+$ $(1s\sigma_g\,2s\sigma_g)$, and $e\ ^3\Sigma_u^+\ (1s\sigma_g\,2s\sigma_u)$. The latter three states constitute to the triplet Rydberg electronic manifold as they correlate to the $2s$ (^{2}S*) and $2p$ (^{2}P*) excited atom asymptotes. Finally, the *ab initio* pair potential data is used in the QMC and DFT calculations, which describe the inhomogeneous liquid interface around the excimer.

A. *Ab initio* potentials

The molecular orbitals, energies, and transition dipole moments are obtained by the ICMRCI (Internally contracted multireference configuration interaction) [23,24] method. This method is used for solving the electronic Schrödinger equation, having the one-electron space discretized in terms of nuclear-centered Gaussian functions of Dunning *et al.* [25]. To describe the excited H atoms, doubly augmented basis set (d-aug-cc-pV6Z; dav6z) is selected as the sufficiently diffuse functions yield the $2s$, $2p$ atomic levels with proper accuracy. The dav6z energy separations $\Delta E_{1s\leftrightarrow 2s}$ and $\Delta E_{1s\leftrightarrow 2p}$ are 10.2055 eV and 10.2068 eV, respectively, while the experimental value is 10.1988 eV [26]. With smaller basis sets of Dunning, which have fewer high angular momentum basis functions, these energy separations become davqz: 10.2055 eV and 10.2080 eV; dav5z: 10.2058 eV and 10.2077 eV. A more notable difference between these basis sets becomes apparent when inspecting the energetics of the $3s$ and $3p$ shells.

Interaction of the ground state He atom with the excited H_2* molecule is computed in a similar way with the dav5z basis set centered on both H and He atoms. Collinear and perpendicular (T-shape) atomic configurations were considered, where in the former the electronic states ^3b, ^3a, and ^3e correspond to the three lowest CI roots in A_1 of C_{2v} point group, and the c state has the B_2 symmetry. For the T-shaped configuration, both ^3a and ^3c belong to A_1 while ^3b and ^3e lie in the B_2 representation. The Rydberg molecule geometry is fixed at internuclear separation of 1.047 Å, which is the average of ^3a and ^3e state equilibrium distances [27]. Reference calculation for the ICMRCI method, MCSCF (state-averaged multiconfiguration self-consistent field) [28,29], employs complete active space (CAS) orbitals. For the four electrons in H_2*-He calculation the active space consists of 10 orbitals in the collinear case and 8 orbitals in the perpendicular case.

The counterpoise correction [30] is used in eliminating the basis set superposition error from all the computed potential energy curves $V_{H_2*\text{-}He}(r)$. Moreover, the obtained en-

ergies are subject to the multireference analogue of the Davidson correction [31,32] in order to approach size-extensive limit at the MRCI stage. While the four electron calculation H_2^*-He does not strictly follow size-extensive behavior, the two-electron fragments in the counterpoise scheme are subject to full CI level treatment, which should affirm on reliability of the correction method. All the electronic structure computations were performed with MOLPRO2002.3 program [33].

B. Density functional method

Our theoretical description of the quantum fluid structure around the solvated H_2^* molecule is based on a density functional proposed by Dupont-Roc *et al.* [17] (Orsay-Paris functional). The energy functional depending on liquid density ρ has the following form:

$$E[\rho(r)] = \frac{\hbar^2}{2M_{He}} \int |\nabla \sqrt{\rho(r)}|^2 d^3r + \frac{1}{2}\int\int \rho(r) V_{LJ}(|r-r'|)\rho(r') d^3r' d^3r + \frac{c}{2}\int \rho(r)\left(\int \rho(r')\Pi_h(|r-r'|)d^3r'\right)^{1+\gamma} d^3r + \int V_{H_2^*\text{-}He}(|R-r|)\rho(r)d^3r, \quad (1)$$

where the model parameters have been calibrated to the compressibility of the bulk superfluid and to reproduce the static polarizability and surface energy at 0 K temperature. The last term introduces interaction of the liquid with a pointlike impurity center located at R. This functional has proven to be reasonably reliable for describing both static and dynamic properties of various liquid helium systems doped with impurities [11,34]. In Eq. (1) the Lennard-Jones interaction potential is screened at short distances:

$$V_{LJ}(r) = \begin{cases} 4\varepsilon\left[\left(\frac{\sigma}{r}\right)^{12} - \left(\frac{\sigma}{r}\right)^{6}\right] & \text{for } r \geqslant h, \\ V_{LJ}(h)\left(\frac{r}{h}\right)^4 & \text{for } r < h, \end{cases} \quad (2)$$

with hard core radius $h = 2.377$ Å and Lennard-Jones parameters: $\varepsilon = 10.22$ K and $\sigma = 2.556$ Å. The spherical averaging function is defined as $\Pi_h(r) = 3(4\pi h^3)^{-1}$ for $r \leqslant h$ and zero elsewhere. The short-range correlation parameters are $c = 10\,455\,400$ K Å$^{3+3\gamma}$ and $\gamma = 2.8$. In order to find the ground state solution, the effective single-particle equation is solved,

$$\left(-\frac{\hbar^2}{2M_{He}}\Delta + U[\rho, r]\right)\sqrt{\rho(r)} = \mu\sqrt{\rho(r)}. \quad (3)$$

This equation is obtained by requiring that energy in Eq. (1) is stationary with respect to variations in liquid density (see, for example, Ref. [11]). Furthermore, we have introduced Lagrange multiplier μ for proper normalization of Eq. (3).

To supply a reasonable initial guess for our numerical calculations as well as to rationalize the obtained results, we employ Jortner's trial function for the liquid profile [14],

$$\rho(r, r_0; \alpha) = \begin{cases} 0 & \text{when } r \leqslant r_0, \\ \rho_0(1 - [1 + \alpha(r - r_0)]e^{-\alpha(r-r_0)}) & \text{when } r > r_0, \end{cases} \quad (4)$$

which contains two variable parameters: bubble edge, r_0, interfacial thickness range, α^{-1}, and ρ_0 is the bulk liquid density (at 0 K and under saturated vapor pressure $\rho_0 = 0.021836$ Å^{-3}). A useful property for spherical bubbles is the mass barycenter of the vacuum-gas-liquid interface ("bubble radius"), which can be obtained approximately from Eq. (4) as $r_b \approx r_0 + 2/\alpha$.

As a higher level of approximation to the density functional, instead of Eq. (1), we have also used an improved functional proposed by Dalfovo *et al.* [18]. This functional includes a nonlocal correlation term to the kinetic energy, which depends on gradients of the density, and yields better description of the static response function in the roton region. Therefore it provides better structural characteristics at interatomic length scale than Eq. (1). Details of the numerical procedure for obtaining stationary solutions of Eq. (3) with the functionals of Eq. (1) and Dalfovo *et al.* [18] have been given elsewhere [11]. It should be pointed out that we do not explicitly consider thermal excitations in these calculations. Strictly speaking this means that the calculations are limited to the 0 K case. However, for the present system such thermal corrections may be crudely included by variation of the bulk density as a function of liquid temperature. In general, thermal fluctuations tend to widen the interface region as shown in Ref. [35]. In the following calculations we use the experimentally known correspondence between the liquid density and temperature to mimic the nonzero temperature.

C. Hybrid DFT/QMC calculations

In cases where the external excimer-helium potential is deeply bound (e.g., ^3c and ^3e states), it was observed that both functionals failed to converge properly within the symmetry dictated by the external potential. The results also indicated excessive liquid localization in the bound parts of the potential. For this reason we have developed a hybrid method consisting of QMC and DFT. When the excimer-He potential is very deeply bound, a number of He atoms separate from the bulk and form a strongly bound H_2^*-$(He)_n$ complex. Initial modeling of this complex was carried out in the gas phase using unguided diffusion Monte Carlo (DMC) utilizing dynamical energy adjustment. Next, DFT calculation step was carried out using an external potential arising from the complex-liquid coupling energy:

$$E[\rho_{H_2^*},\rho_{He_{frozen}},\rho_{He_{bulk}}]=\int\int \rho_{H_2^*}(r)V_{H_2^*\text{-}He}(|r-r'|)(\rho_{He_{frozen}}(r')+\rho_{He_{bulk}}(r'))d^3r'd^3r + \int\int \rho_{He_{frozen}}(r)V_{He\text{-}He}(|r-r'|)\rho_{He_{bulk}}(r')d^3r'd^3r, \quad (5)$$

where $\rho_{H_2^*}$, $\rho_{He_{frozen}}$, and $\rho_{He_{bulk}}$ are the densities for the H_2^* excimer, He atoms in the complex, and He atoms in the bulk, respectively. For the He-He interaction $V_{He\text{-}He}$ we have used the potential of Aziz *et al.* [36] without any short-range correlation terms. The second step of iteration consisted of guided DMC calculation for the complex with external potential due to liquid [Eq. (5)]. For ^3c state excimer four ground state He atoms (i.e., $n=4$) are bound to it in a ring structure around the Rydberg orbital (see Fig. 2). The DMC trial wave function is then written as

$$\psi_{trial}(r_{H_2^*},r_{He_1},\ldots,r_{He_n}) = \psi_{H_2^*,xy}(r_{H_2^*})\psi_{H_2^*,z}(r_{H_2^*})\prod_{i=1}^{n}\psi_{He,xy}(r_{H_2^*},r_{He_i}) \times \psi_{He,z}(r_{H_2^*},r_{He_i})\prod_{i<j}^{n}\psi_{He,He}(r_{He_i},r_{He_j}), \quad (6)$$

$$\psi_{H_2^*,xy}(r)=e^{-(1/2)B^2(x^2+y^2)}, \quad \psi_{H_2^*,z}(r)=e^{-(1/2)C^2z^2},$$

$$\psi_{He,xy}(r,r_i)=e^{-(1/4)\alpha^4(d_i-R_\alpha)^4-(1/2)\beta^2(d_i-R_\beta)^2},$$

$$\text{where } d_i=\sqrt{(x-x_i)^2+(y-y_i)^2},$$

$$\psi_{He,z}(r,r_i)=e^{-(1/2)\gamma^2(z-z_i)^2},$$

$$\psi_{He,He}(r_i,r_j)=e^{-(1/8)(q/|r_i-r_j|)^8},$$

where $\alpha=1.6$, $\beta=1.6$, $\gamma=2.3$, $R_\alpha=3.5$, $R_\beta=2.5$, $q=4.5$, $B=1.5$, and $C=1.5$ are variational parameters expressed in a.u. The symmetry axis in Eq. (6) was defined along z. Terms that approximate the excimer-helium and helium-helium interactions depend only on the internal coordinates whereas the excimer part depends only on the external origin that is defined by the surrounding liquid. The latter models the zero-point motion of the complex residing inside the solvation cavity. Without translational degrees of freedom the trial function of Eq. (6) provides $\sim$95% of the unguided DMC energy. Overall the hybrid DFT/QMC calculation consists of multiple iterations between the QMC and DFT models, which will provide proper feedback between the complex and the liquid. Such iterations were repeated few times in order to verify proper convergence. It should be noted that values for variational parameters B and C in Eq. (6) were obtained during this iteration process. Finally, we note that the applied pure DMC and importance sampled DMC algorithms follow closely those described in Ref. [37].

The *ab initio* electronic structure and one-dimensional self-consistent field based DFT calculations [11,13] were carried out using Linux PCs whereas the hybrid QMC and 3D DFT imaginary time propagation-method calculations [38] were computed with IBM pSeries 690 parallel computer using 8 processors.

III. RESULTS

A. Diatomic H_2^* excimer

The potential energy curves for the calculated H_2^* $b\ ^3\Sigma_u^+$, $c\ ^3\Pi_u$, $a\ ^3\Sigma_g^+$, and $e\ ^3\Sigma_u^+$ states are shown in Fig. 1. These graphs show that, in contrast to the He_2^* where the $a\ ^3\Sigma_u^+$ state is metastable, the lowest H_2 triplet state $b\ ^3\Sigma_u^+$ is repulsive and provides dipole allowed transition from the $a\ ^3\Sigma_g^+$ and above gerade Rydberg states [39,40]. Transition from nearly degenerate $c\ ^3\Pi_u$ state (dashed curve in Fig. 1) to $b\ ^3\Sigma_u^+$ is parity forbidden.

We present the radiative lifetimes (τ) of the ^3e state vibronic levels in Table I, as obtained by numerical integration of the nuclear Schrödinger equation and subsequent Franck-Condon analysis according to the Fermi golden rule. The resulting radiative gas-phase lifetime for the $e\ ^3\Sigma_u^+$ state $v'=0$ level is 30.2 ns, with transition energy $\nu_{00}=11558.9\ \text{cm}^{-1}$ deviating by 0.4 % from the experimental value of 11605.7 cm^{-1} [27]. Table II lists our computed transition origins ($J'=J''=0$) for those (ro-)vibronic transitions which were detected in the liquid He experiment [7]. The comparison is made against the gas phase values [27], while in the liquid these lines are blue-shifted between 2 and 11 cm^{-1} [7]. Our calculated transition probabilities for

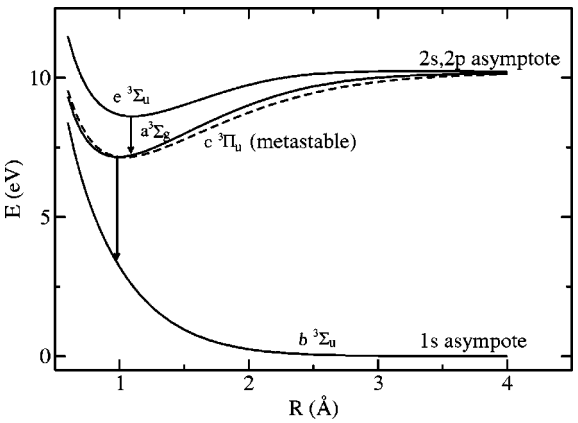

FIG. 1. Potential energy curves for the lowest four triplet states of H_2 as obtained from ICMRCI/d-aug-cc-pV6Z calculation. The zero of the energy is at the free ground state H atom asymptote.

TABLE I. The computed gas-phase transition probabilities $A_{v'v''}$ for the $^3e(v')\rightarrow{}^3a(v'')$ system, and the resulting radiative lifetimes $\tau_{v'}=(\Sigma_{v''}A_{v'v''})^{-1}$. $x[y]=x\times10^{y}$.

	$A_{v'v''}$ (s^{-1})				
v''/v'	0	1	2	3	4
0	2.88[7]	7.83[6]	1.75[6]	3.90[5]	8.94[4]
1	4.22[6]	1.54[7]	1.05[7]	3.86[6]	1.23[6]
2	1.01[5]	6.74[6]	6.91[6]	9.87[6]	5.39[6]
3	3.48[2]	2.91[5]	7.83[6]	2.14[6]	7.40[6]
4	7.72[−2]	1.68[3]	5.59[5]	7.70[6]	1.80[5]
5	1.06[−7]	7.93[−1]	5.21[3]	8.87[5]	6.56[6]
6		9.18[−8]	5.00[0]	1.33[4]	1.24[6]
7			7.54[−5]	2.57[1]	3.04[4]
8				3.61[−3]	1.23[2]
9					8.14[−2]
τ (ns)	30.2	33.0	36.3	40.2	45.2

$^3a\leftrightarrow{}^3c$ and $^3a\leftrightarrow{}^3b$ are very close to the previously reported values of Dalgarno *et al.* [41,42]. Furthermore, we note that the calculated transition moment matrix elements $\langle e|\mathbf{r}|a\rangle$, $\langle a|\mathbf{r}|b\rangle$, and $\langle a|\mathbf{r}|c\rangle$ are nearly identical to those obtained with explicitly correlated variational electronic wave functions [43].

In this work we are concerned with the optical $^3e\rightarrow{}^3a$ transition, the only one reported in the experimental work of Trottier *et al.* [7], and study the solvation cavity structures of these two electronic states within the liquid. To show the spatial extents and symmetries of the related Rydberg electron wave functions, we present the natural orbital contour plots in Fig. 2. The clear difference between the two states is that, while the electron density in the ^3a state is nearly spherical far from the ionic core, the ^3e state possesses an angular node due to antibonding combination of $2s$ atomic orbitals. Both of the states exhibit a radial node in the electron density at close distances.

B. Triatomic H_2^*-He

The interaction between a single ground state He atom and the H_2^* excimer can be approximately described in terms of two competing effects: Pauli repulsion between the Rydberg electron and closed shell electrons of the He atom, and polarization attraction arising from the ionic H_2^+ core. Evidently, the latter contribution is efficiently shielded in the spherical ^3a state, whereas for the ^3e, ^3b, and ^3c states attraction arising from the polarization interaction is strong. This means that an anisotropic electron distribution will lead to strongly anisotropic potential with strongly repulsive as well as deeply bound parts. To quantify these expectations, we have chosen to compute the collinear (L) and perpendicular (T) approaches of the ground state atom with respect to molecular axis of the excimer. As the anisotropic Rydberg orbitals closely resemble atomic p orbitals, it is a good approximation to construct the whole potential energy surface from trigonometric interpolation (see, for example, Ref. [11]). Computation of the full potential energy surface by *ab*

TABLE II. Selected transition energies $\nu_{v'v''}$ (cm^{-1}) for the computed $^3e\rightarrow{}^3a$ system are shown. The experimental gas phase values are calculated from the P-branch rotational lines as $\nu_{v'v''}=\nu_{P1}+2B_{v''}$. Gas phase data were obtained from Ref. [27].

Transition ($v'-v''$)	Calculated	Experiment in gas phase
(2-3)	8391.8	8426.4
(1-2)	8714.0	8755.5
(0-1)	9035.1	9081.3
(1-1)	11100.4	11144.0
(0-0)	11558.9	11605.7
(3-2)	12436.8	
(2-1)	13030.9	
(1-0)	13624.1	

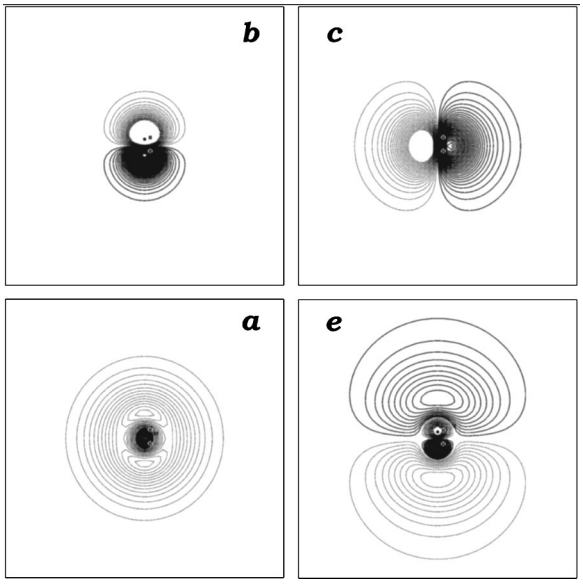

FIG. 2. The ICMRCI/davqz calculated natural orbital plots of H_2 triplet states $b\ ^3\Sigma_u^+$, $c\ ^3\Pi_u$, $a\ ^3\Sigma_g^+$, and $e\ ^3\Sigma_u^+$ at the internuclear separation of 1.047 Å. The box dimension is $40a_0\times40a_0$ and the contour level step is 0.0025 in each graph.

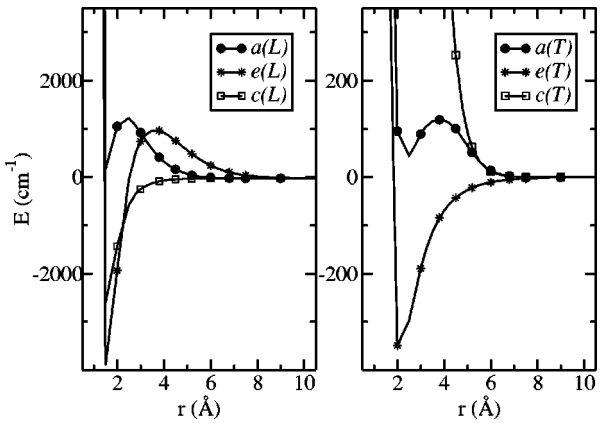

FIG. 3. The panels have been labeled as left: potential energy curves for H_2*-He at collinear geometry; right: potential energy curves for H_2*-He at T-shape geometry. The state labels ^3a, ^3e, ^3c are for the H_2 molecule fixed at 1.047 Å internuclear separation, and the He atom distance r is measured from the H_2* mass center.

initio is out of the question due to loss of molecular symmetry. The resulting potential energy curves, $V_{H_2*\text{-}He}(r)$, for the three electronic states (^3a, ^3c, and ^3e) are shown in Fig. 3. The calculated energies of the triatomic configurations are collected in Table III for ^3a and ^3e states. In the collinear approach, both of these states are repulsive until a radial node in the electron density yields an inner well. Far away from the excimer core the interaction is nearly isotropic for the ^3a state. On the other hand, in the perpendicular geometry of the ^3e state an angularly sharp potential minimum occurs with depth of $\sim 350\ \text{cm}^{-1}$. The situation resembles that of the closely related He_2*-He (^3a, ^3c) system [22]. Because the positive core is shielded only by one electron in H_2* the potential wells appear deeper. A closer view on the long-range part of the potentials relevant to the H_2* bubble formation is provided in Fig. 4, where spherical average has been taken from the potentials of Fig. 3. These spherical potentials will be applied later in the DFT calculations as the

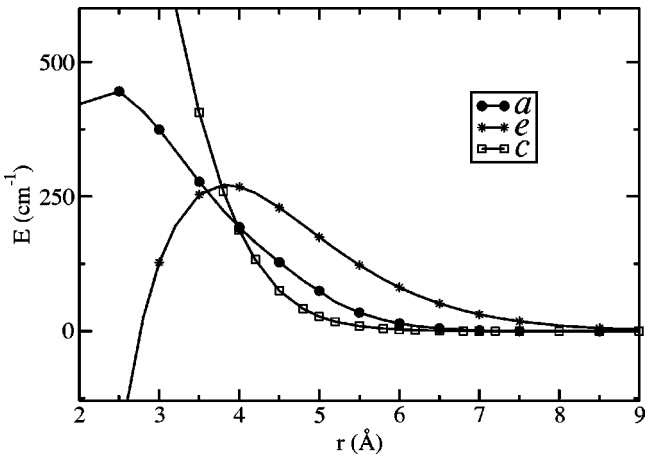

FIG. 4. Angularly averaged (radial) potential energy curves for H_2*-He representing long-range interaction of freely rotating excimer (cf. Fig. 3).

TABLE III. Computed potential energies $V_{H_2*\text{-}He}(R)$ in cm^{-1}, based on ICMRCI/dav5z level of theory, for $a\ ^3\Sigma_g^+$ and $e\ ^3\Sigma_u^+$ states of H_2*, approached in a collinear (L) or broadside (T) manner by ground state He atom.

R (Å)	a (L)	a (T)	e (L)	e (T)
1.0	49179.41	10463.25	43596.05	11216.87
1.5	186.20	1340.06	−3874.30	812.81
2.0	1074.28	95.21	−1914.29	−348.88
2.5	1248.23	44.08	−29.71	−298.06
2.8	1084.90	69.20	539.92	−232.92
3.0	944.68	89.24	762.24	−189.88
3.2	801.09	103.52	893.52	−154.64
3.5	601.17	115.52	989.04	−114.12
3.8	434.13	118.92	984.31	−84.77
4.0	343.41	117.34	944.14	−69.75
4.2	268.54	112.88	884.72	−57.50
4.5	182.46	100.66	774.73	−43.16
4.8	122.14	79.05	655.55	−32.48
5.0	93.05	65.00	577.19	−26.92
5.2	59.28	51.11	502.65	−22.32
5.5	35.93	33.12	401.14	−16.91
5.8	21.05	19.97	314.10	−12.86
6.0	14.40	13.74	264.35	−10.73
6.2	9.61	9.15	220.96	−8.97
6.5	4.92	4.61	166.88	−6.90
6.8	2.19	1.98	124.40	−5.34
7.0	1.09	0.92	101.58	−4.52
7.2	0.35	0.24	82.51	−3.85
7.5	−0.27	−0.34	59.84	−3.05
8.0	−0.61	−0.63	34.19	−2.12
8.5	−0.60	−0.59	18.95	−1.53
9.0	−0.48	−0.47	10.17	−1.15
9.5	−0.33	−0.32	5.26	−0.45
10.0	−0.22	−0.22	2.59	−0.29
12.0	0.00	0.00	0.00	0.00

experiments suggest near free rotation of the ^3e state H_2* molecule in liquid helium [7].

As the DFT calculations involve many He atoms, it is necessary to see if the above *ab initio* potentials are pairwise additive. To model the many-body effects we have performed four-atom MRCI calculations (e.g., He-H_2*-He). Instead of one He atom approaching the H_2* center, the interaction of two atoms symmetrically located in perpendicular or collinear fashion was recorded as a function of their separation, and then divided by two. For purely pairwise additive interaction this should yield equal results to the three-atom calculation provided that the He(^{1}S)-He(^{1}S) interaction is small. It was observed that the triatomic potential shapes with wells and barriers (cf. Fig. 3) even at close distances were reproduced by the four-atom calculations. Thus we conclude that the many-body effects in the present case are negligible. In all previous calculations the H_2^+ core bond length was held fixed. In cases where the ground state He atom approaches the excimer core to close distances, we have car-

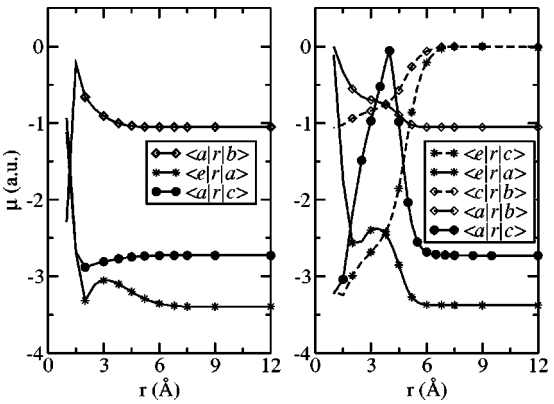

FIG. 5. The H_2^* transition dipole moments for collinear (left panel) and T-shaped H_2^*-He (right panel) configurations. The near degeneracy of ^3a and ^3c states is seen in crossings at short perturber distances, although the root flip occurs already at 4.8–5.0 Å.

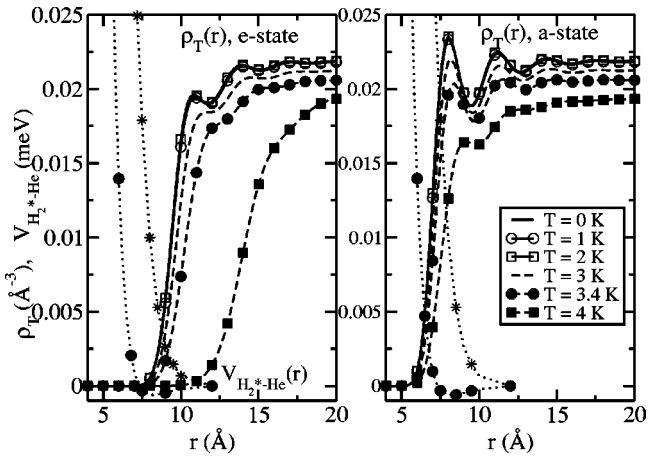

FIG. 6. The temperature dependent He density profiles $\rho_{\mathrm{He}}(r)$ around ^3e-state (left panel) and ^3a-state (right panel) impurities are shown. The spherically averaged interaction potentials $V_{H_2^*\text{-}He}(r)$ are also shown, the more repulsive belonging to the ^3e state and the other for ^3a. This calculation employs the functional of Dalfovo *et al.* [18].

ried out geometry optimization within the C_{2v} symmetry. In these calculations the excimer core structure was not broken and therefore there is no need to consider decomposition of the excimer provided that the C_{2v} symmetry is conserved.

In addition to energetics, the approaching He atom will also modify the electronic transition dipole moments between the states. The transition moments as a function of the excimer-He distance are plotted in Fig. 5. It can be seen that the $\langle e|\mathbf{r}|a\rangle$ matrix element stays practically constant far away from the excimer whereas large changes occur at short distances. Thus the oscillator strengths and radiative lifetimes of the H_2^* molecule are not markedly affected when the He atom remains far away from the ionic core. On the other hand, if the He atom can penetrate into nodal planes of the Rydberg electron, the radiative lifetimes will be strongly affected. This can be seen, for example, from the distance dependency of the $\langle e|\mathbf{r}|a\rangle$ matrix element in the right panel of Fig. 5.

Of particular interest is metastability of the ^3c state with respect to ^3a, where the population can leak to as seen from the transition moment calculations and Fig. 1. As these states are almost degenerate, the approaching ground state He atom can alter their relative energetics dramatically. Especially in the collinear geometry, if a ground state He atom approaches close to the excimer core then the total energy for the ^3a state increases whereas for the ^3c state it decreases. This will have important implications to the stability of the ^3c state solvated in liquid helium as will be discussed later. A similar situation was observed for some strongly bound states of the He_2^* as documented in Ref. [11].

C. Density functional calculations of the bubble structure

As a first approximation we consider the ^3a and ^3e states to be isotropic by calculating their spherically averaged interaction potentials as $V_{iso}(r)=[V_{linear}(r)+2V_{T\text{-}shape}(r)]/3$ and then carrying out the DFT calculation in spherical coordinates (i.e., 1D model). This approach assumes free molecular rotation in both electronic states of the excimer. In the experiment the rotational structure was resolved for several vibronic bands, (2-3), (1-2), (0-1), (1-1), (0-0), (3-2), (2-1), and (1-0), and with the $P(1)$ line most intense in every case. In other words, the $J'=0$ rotational level of ^3e state was preferentially populated with estimated rotational temperature of 35 K [7]. As the experiments were carried out at temperatures above the λ point, between 3.0–4.2 K, comparison with our 0 K DFT calculation is not exact. We have, however, taken the nonzero liquid temperature into account only approximately by adjusting the ^{4}He bulk density ρ_0. The resulting density profiles as a function of temperature are presented in Fig. 6, where the calculations employed the improved energy functional of Dalfovo *et al.* [18]. The density profile remains essentially unchanged at temperatures between 0–2 K, i.e., below the λ point, as a direct consequence of the bulk density remaining constant in this temperature range. It is important to notice that the cavity formation is very sensitive to the H_2^*-He interaction potential at long range since the bubble edge is generated as a response to the perturbation of only few cm^{-1} in magnitude. We present the bubble parameters, which were obtained by least squares fitting the Jortner's trial function of Eq. (4) to the calculated profiles, in Table IV.

For freely rotating ^3c state excimer we obtain the excimer-liquid interaction by taking spherical average of the anisotropic H_2^*-He pair potentials. The resulting liquid sol-

TABLE IV. Cavity size parameters for spherical bubbles around ^3e and ^3a state excimers, obtained by fitting the Jortner function Eq. (4) to the density profiles calculated with Dalfovo-Stringari functional, and shown in Fig. 6.

T (K)	0–2	3.0	3.4	4.0
$r_b(e)$ (Å)	9.71	10.1	10.7	14.5
$\alpha(e)$ ($\mathrm{Å}^{-1}$)	1.27	1.08	0.91	0.73
$r_b(a)$ (Å)	6.92	7.04	7.21	7.99
$\alpha(a)$ ($\mathrm{Å}^{-1}$)	2.93	2.53	2.06	1.05

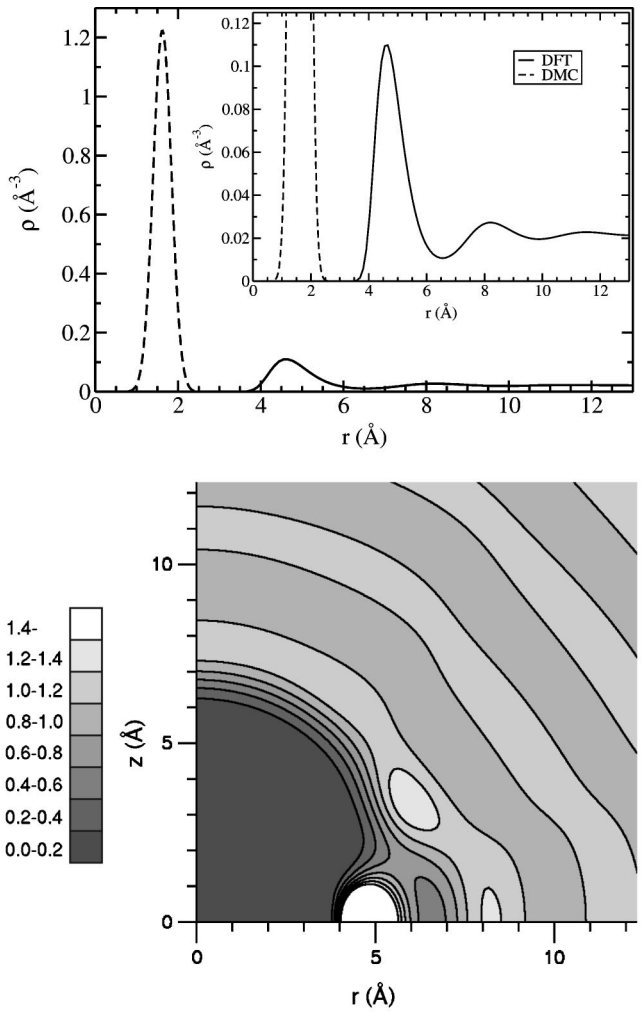

FIG. 7. Liquid ^{4}He density around the rotationally quenched H_2^* (^3c) excimer is shown. The calculation corresponds to the hybrid DFT/QMC calculation using the functional of Dalfovo *et al.* [18] with a spatial step size of 0.1 Å. Top: cut along the axis perpendicular to the Rydberg orbital is shown; bottom: contour plot of the DFT liquid density is shown in units of ρ_0.

vation structure is very similar to the ^3a state but with $r_b \sim 6.3$ Å. However, the situation is quite analogous to the He_2^* system (see Ref. [11]) and thus this solvation form may not be stable. If the rotational motion would partially quench, the resulting structure would be quite complicated and will not be considered here. If the molecular rotation is completely quenched in the ^3c and ^3e states then the anisotropic excimer-liquid potential breaks the spherical symmetry in Eq. (3). Both states exhibit strongly bound regions in their pair potentials, which are many orders of magnitude larger than the average energy of single helium atom (ca. -7 K/atom) in the liquid. Due to complications in the ^3e state potential shape, we have not attempted to carry out the calculations for this state. Even for rotationally quenched ^3c state both DFT models (Orsay-Paris and Dalfovo *et al.* [18]) failed to converge to physically meaningful results (e.g., solutions with excessive liquid localization). For this reason the strongly bound parts were treated separately by using DMC.

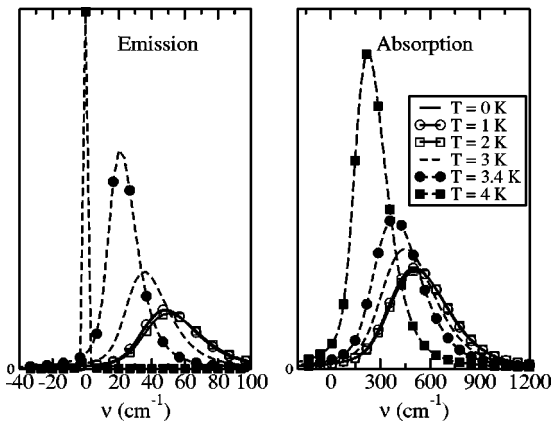

FIG. 8. The emission ($^3e \rightarrow {}^3a$) and absorption ($^3e \leftarrow {}^3a$) spectra of an embedded H_2^* molecule, dictated by H_2^*-He potential energy differences and ^{4}He-density profiles at different liquid densities. The narrow bands at the lowest density have been scaled down to fit the image. The wave number indication refers to shifts of the transition from the unperturbed gas-phase value. Liquid density profiles in the line shape calculations were obtained using the functional of Dalfovo *et al.* [18].

By carrying out DMC calculations for the subsystem containing the excimer and the localized He atoms (''belt atoms''), the following total energies were obtained: $(n=3)$ -9520 ± 100 K and $(n=4)-11830\pm70$ K. In cases where $n>4$ the DMC calculations indicated that He atom density would leak beyond the H_2^*-He potential minimum. The four-atom cluster $(n=4)$ yielded the lowest energy and thus we have used the one particle density from this calculation in constructing the initial effective potential for DFT. The resulting liquid density profile from the iterated hybrid DMC/DFT calculation is shown in Fig. 7.

D. Electronic spectra

We proceed to simulation of emission and absorption spectra using the Dalfovo-Stringari functional [18] for evaluation of the liquid density $\rho(r)$, and calculating the optical line shape via time dependent perturbation theory [44,45]. The general formula for dipolar spectrum between two electronic states is given by

$$I(\omega) \cong \int c(t) e^{i\omega t} dt, \tag{7}$$

where the line shape function $I(\omega)$ is written as Fourier transform of the dipole time-correlation function $c(t)$. With the quite commonly used [11,46] Anderson expression [47,48],

$$c(t) = e^{-\int [1 - e^{-i\Delta V_{fi}(r)t/\hbar}] \rho_i(r) d^3 r}, \tag{8}$$

we can determine the spectra with a known liquid density profile on the initial state, and the continuum of frequencies generated by the difference potential $\Delta V_{fi}(r) = V_f(r) - V_i(r)$. This formulation has its origin in the gas phase pressure induced broadening of electronic transitions. In the present case most effects originate from the gas part of the

TABLE V. Spectral widths and line shifts for the $^3e \leftrightarrow {}^3a$ transitions of H_2^* in liquid He, obtained by Eq. (6) using He density profiles calculated for different temperatures.

T (K)	0–2	3.0	3.4	4.0
ρ_0 ($Å^{-3}$)	0.0218	0.0212	0.0206	0.0193
Emission				
Width (cm^{-1})	40	30	20	<5
Shift (cm^{-1})	50	35	20	0
Absorption				
Width (cm^{-1})	425	385	335	230
Shift (cm^{-1})	510	445	380	225

liquid profile and therefore this form of time correlation function is expected to be a good approximation. Furthermore, no structure due to liquid motion is expected to be visible in the lines as the transitions are broad. Such structured spectra cannot be, in general, simulated using Eq. (8) [49]. The applied density profiles are plotted in Fig. 6, and we show the results of the spectral line shape evaluation in Fig. 8. Broadening of the lines as the temperature decreases, and the pronounced blue shift of the peak positions respectively, are clearly produced as a straightforward outcome of the calculations. We collect the spectral predictions in Table V.

IV. DISCUSSION

A. Electronic structure calculations

The gas phase *ab initio* calculations of H_2^* were carried out in order to validate our methods against the existing data. With this respect our *ab initio* calculations are in good agreement with the existing experimental and theoretical results as outlined in the Results section and summarized in Fig. 1 and Table II. Experimental data on radiative lifetimes (see Table I) for the ^3e state appears not be available. This is probably due to the fact that there is no easy way to prepare the ^3e state in a controlled fashion for subsequent measurement of the radiative lifetime. An expected general trend is that the electronic states of H_2^* excimer closely resemble to those of the He_2^* molecule [22]. The main difference is that the ^3b state in H_2^* is purely repulsive and leads to permanent dissociation. For this reason the H_2^* ^3a state is not metastable whereas in the He_2^* this state exhibits metastability. In the latter case the metastability arises from negligibly small spin-orbit interaction and the absence of any repulsive triplet states below it. However, the ^3c state of H_2^* is metastable as observed by both experiments [50] and theory [51] in the gas phase. Furthermore, as a Π state it carries double degeneracy with, for example, Cartesian components $\Pi_{x,y}$. In cases where cylindrical molecular symmetry around the molecular axis is broken, this state splits into two energetically unequivalent components. This is analogous to crystal field splitting of a Π state molecule.

It is known from previous studies (see Refs. [11,22]), that the interaction between a spherical Rydberg state excimer with a ground state He atom is approximately described by Pauli repulsive forces. When such forces are absent, deep penetration of the ground state He atom towards the charged excimer core is possible. Based on these considerations, it is possible to obtain qualitative expectations for the pair interaction between the H_2^* excimer and a ground state He atom. As shown in Fig. 2 the Rydberg electron wave function depends strongly on the electronic state of the excimer. Thus we should expect that spherically symmetric states (e.g., ^3a) without any far-reaching nodes would display nearly spherically symmetric interaction potential without any deeply bound part. The only possible source for binding arises from the long-range dispersion forces. All the other states except ^3a have angular nodes in their Rydberg wave functions. If the ground state He atom would enter these nodal regions then the Pauli repulsion would be effectively cancelled. For example, the ^3e state has complicated Rydberg electron wave function (resembling a $2p$ atomic orbital) as it has both angular and radial nodes. The ^3c state, on the other hand, has only an angular node along the diatomic axis but there is an additional complication due to degeneracy factor arising from the orbital angular momentum. All these qualitative expectations are confirmed by our *ab initio* calculations as summarized in Figs. 2 and 3. The ^3a state is closely spherically symmetric with almost exclusively repulsive interaction. At short distances there is a turn over in the potential when the charge imbalance between the excimer core and the Rydberg electron temporarily decreases the potential. This leads to a small dip in the potential at ca. 1.5 Å. In the ^3c state repulsive interaction occurs only when the Rydberg Π (Cartesian) orbital is locked towards the approaching ground state He atom. In all other cases the H_2^+ core induces strong binding via polarization of the approaching He atom. If the Rydberg orbital is locked in space, the excimer will have deeply bound (ca. 2600 cm^{-1}) ''donut''-like region around the neck of the Rydberg p-like orbital. Finally, the many-body effects were evaluated with two ground state He atoms approaching the excimer. Based on these calculations we have concluded that the many-body contribution is small. The many-body effects are expected to be significant only in cases where small Rydberg electron densities extend far away from the excimer core. An example of such case is provided by the He_2^* ^3d state [22]. In addition to energetic considerations, the approaching ground state He atom affects the transition dipole moments between the states as shown in Fig. 5. For example, in the ^3e state, penetration of the ground state He atom to the excimer core region decreases the transition dipole moment significantly.

B. DFT/QMC calculations

For spherical ^3a and spherically averaged ^3c and ^3e states Eq. (3) can be solved in spherical coordinates. The results for ^3a and ^3e states are shown in Fig. 6. Here the pair potential is mainly repulsive for both electronic states, apart from a small attractive dispersion interaction, as shown in Fig. 4. In such cases the vacuum-gas-liquid interface is expected to be rather smooth with small oscillations in density due to correlated nature of the liquid and weak bound region between the excimer and the liquid. For such systems the

Jortner's trial function is expected to give reasonable representation of the liquid density. Obviously any density oscillations or curvature close to the excimer cannot be properly described by this function. Both applied DFT functionals gave comparable liquid density profiles, with the main difference occurring in the liquid density oscillations at the interface. When the bulk helium density corresponds to saturated vapor pressure at 0 K, the H_2^* (^3a) and H_2^* (^3e) excimers form spherical bubbles in the liquid with radii of 6.9 Å and 9.7 Å, respectively. Both values are slightly smaller than the ones obtained from the experiments and bubble model analysis of Trottier *et al.* [7] [$r_b(a) \sim 8$ Å and $r_b(e) \sim 11$ Å]. With the liquid density adjusted to correspond to 4 K temperature, the calculated bubble radii expand to 8 Å and 14 Å for ^3a and ^3e states, respectively (see Fig. 6). For ^3a state the calculated bubble radius coincides with the result of Ref. [7] whereas the ^3e state radius appears to be larger. Overall our *ab initio* and DFT based calculations yield comparable results to those obtained from the bubble model with experimental guidance. However, in order to carry out direct comparison against experimental data, we will evaluate spectroscopic features involved in the $^3e \leftrightarrow {}^3a$ transition later in the text.

The ^3c state excimer demonstrates variety of possibilities for solvation in liquid helium. Three different schemes are possible: (1) bare excimer with free rotation (i.e., spherical object), (2) complicated intermediate form, where molecular rotation and/or Π-orbital degeneracy are partially quenched, and (3) completely quenched excimer-He complex (i.e., the belted complex). Each of these forms should represent a local energy minimum, thus method of preparation and the energy barriers that connect the minima will dictate which form will actually be seen in the experiments. Case (1) remains in spherical cavity where $r_b \sim 6.3$ Å. Sufficiently strong asymmetric liquid motion will destroy this state (e.g., thermal perturbations or preparation process). Possible transition between cases (1) and (2) involves a dynamical barrier which depends on a delicate balance between the attractive H_2^*-He potential and the kinetic energy tax paid for forcing curvature on the liquid interface. This transition may be spontaneous or it may require external forces to proceed. In case (3) it is not *a priori* clear how many He atoms should enter the bound region (''belt'') of the potential. The minimum energy configuration was reached with four atoms in a beltlike cylindrically symmetric structure around the neck of the Rydberg p-type orbital. The number of atoms present appears very similar to that obtained for He_2^* in Ref. [11]. After formation of the four-atom complex, anisotropic liquid cavity is formed with a clear signature of the secondary solvation structure (see Fig. 7). In both cases (2) and (3) the complex formation will have strong tendency to stabilize the ^3c over the ^3a state and should therefore increase its metastability. Finally, we note that the ^3c state has close analogy to the ^3b state of the He_2^* excimer [11].

C. Spectroscopy

Our line shape calculations include the time correlation function in an approximate fashion as described by Anderson [47] [cf. Eq. (8)]. Exact evaluation of the time correlation function would require full time propagation of both electronic and nuclear wave functions [49]. In the present case the Anderson formula is very convenient to use because it requires only the interaction potentials between the excimer and the liquid in ground and excited states and the initial liquid density profile around the excimer. The time propagation of the system is completely embedded in the approximate time correlation function. Furthermore, in the previous He_2^* study it has been found to give good results [11,46].

First we consider the rotationally resolved $^3e \rightarrow {}^3a$ emission lines, which were observed experimentally [7]. According to Fig. 8, the emission line blue shifts relative to the gas phase position and the overall line shape is almost independent of temperature below the λ-point of liquid helium. Above 2.1 K the emission spectrum rapidly begins to shift towards the gas phase origin because the bulk liquid density decreases. Hence, from the experimental point of view, it would be desirable to carry out such measurements below the λ-point. Furthermore, boiling of the liquid allows for possibility of excimer trapping inside large gas bubbles, which could complicate interpretation of the experimental results. The experimental emission line shifts at 4.2 K are only a few wave numbers, in the range from 2 to 11 cm^{-1} depending on the rotational line. Our calculations predict a line shift ca. 4 cm^{-1}, which is a reasonable accuracy provided that we do not consider molecular rotations and vibrations in our model. Radiative lifetime of the ^3e state is not markedly altered by the surrounding liquid (see Fig. 5) unless parts of liquid would penetrate close to the excimer core. In this case the radiative lifetime should be considerably longer than in the gas phase. In some studies, increase in a radiative lifetime has been used in determining the solvent liquid-impurity interactions (for example, Ref. [52]). In contrast to the emission spectrum, the calculated absorption line experiences (see Fig. 8) much stronger spectral shifting and broadening. These effects originate from strong overlap of the liquid with the Rydberg electron in the upper ^3e state. In general, this demonstrates the well-known fact that the absorption lines are more sensitive to the liquid helium perturbation effects than emission lines. However, in this case the ^3a state is not metastable and therefore such absorption experiment will be difficult to carry out.

In the gas phase the ^3c state has been observed to be metastable [50,51]. However, the situation is not clear in the liquid because this electronic state may exist in various forms of solvation as discussed earlier. If molecular averaging (rotation and orbital degeneracy) persists and the liquid kinetic energy tax is able to keep the liquid from localizing, then this state should remain in spherical cavity [case (1)]. In this case the spherically averaged potential of the ^3a state is more repulsive than the ^3c, and therefore the liquid will energetically slightly favor the ^3c state. In all other cases complex formation will again strongly favor the ^3c state over ^3a. Overall, we can conclude that the surrounding liquid should increase metastability of the ^3c state and as such it should be a good candidate for absorption studies in liquid helium. In the present case the solvent perturbations are very strong for the complexed forms and we have not attempted

to simulate their absorption or emission spectra. Even small changes in the solid ^{4}He layer structure near the excimer core or uncertainty in the repulsive parts of the pair potentials will induce large changes in the calculated optical spectra. A systematic experimental study of such strong spectral shifts was recently carried out by Yabuzaki *et al.* [53]. They were able to study spectroscopically the localization of He atoms in the nodal plane of excited ^{2}P state alkali metal atoms as a function of the He gas pressure.

V. CONCLUSIONS

Our numerical simulations give general suggestions for new experiments on H_2^* excimers in liquid helium. First, in order to maximize the perturbative effects of the liquid and avoid the liquid boiling, the experiments should preferably be carried out below the λ point. Both absorption and emission spectra will then yield larger spectral shifts as well as line broadening effects. In general, absorption measurements will experience stronger impurity-liquid interaction and hence more information of the surrounding helium bath may be obtained than from emission measurements. However, because tightly bound H_2^*-$(He)_n$ complexes may form, a broad spectral wavelength range should be recorded in the spectroscopic experiments. Furthermore, in such case the spectral lines will most likely be very broad. Finally, the metastable ^3c should provide a good way to carry out absorption measurements for the H_2^* excimer in superfluid helium. Due to its various possibilities for solvating in helium, it should provide an excellent candidate for studying the structure of the surrounding solid helium layers and the liquid in highly confined geometries.

ACKNOWLEDGMENTS

This research was partly funded by the graduate school LASKEMO. Computer facilities were provided by the Finnish Center for Scientific Computing (CSC).

[1] J. P. Toennies and A. F. Vilesov, Annu. Rev. Phys. Chem. **49**, 1 (1998).
[2] V. Ghazarian, J. Eloranta, and V. A. Apkarian, Rev. Sci. Instrum. **73**, 3606 (2002).
[3] J. Jortner, L. Meyer, S. A. Rice, and E. G. Wilson, Phys. Rev. Lett. **12**, 415 (1965).
[4] J. W. Keto, F. J. Soley, M. Stockton, and W. A. Fitzsimmons, Phys. Rev. A **10**, 887 (1974).
[5] J. W. Keto, F. J. Soley, M. Stockton, and W. A. Fitzsimmons, Phys. Rev. A **10**, 872 (1974).
[6] V. B. Eltsov, S. N. Dzhosyuk, A. Ya. Parshin, and I. A. Todoshchenko, Low Temp. Phys. **110**, 219 (1998).
[7] A. Trottier, A. I. Jirasek, H. F. Tiedje, and R. L. Brooks, Phys. Rev. A **61**, 052504 (2000).
[8] J. L. Persson, Q. Hui, M. Nakamura, and M. Takami, Phys. Rev. A **52**, 2011 (1995).
[9] E. A. Popov, J. Eloranta, J. Ahokas, and H. Kunttu, Low Temp. Phys. **29**, 510 (2002).
[10] A. V. Benderskii, R. Zadoyan, N. Schwentner, and V. A. Apkarian, J. Chem. Phys. **110**, 1542 (1999).
[11] J. Eloranta, N. Schwentner, and V. A. Apkarian, J. Chem. Phys. **116**, 4039 (2002).
[12] A. V. Benderskii, J. Eloranta, R. Zadoyan, and V. A. Apkarian, J. Chem. Phys. **117**, 1201 (2002).
[13] J. Eloranta and V. A. Apkarian, J. Chem. Phys. **117**, 10139 (2002).
[14] K. Hirioke, N. R. Kestner, S. A. Rice, and J. Jortner, J. Chem. Phys. **43**, 2625 (1965).
[15] E. P. Gross, Nuovo Cimento **20**, 454 (1961).
[16] L. P. Pitaevskii, Sov. Phys. JETP **13**, 451 (1961).
[17] J. Dupont-Roc, M. Himbert, N. Pavloff, and J. Treiner, J. Low Temp. Phys. **81**, 31 (1990).
[18] F. Dalfovo, A. Lastri, L. Pricaupenko, S. Stringari, and J. Treiner, Phys. Rev. B **52**, 1193 (1995), and references therein.
[19] D. M. Ceperley, Rev. Mod. Phys. **67**, 279 (1995), and references therein.
[20] J. Dupont-Roc, Z. Phys. B: Condens. Matter **98**, 383 (1995).
[21] J. Jortner, N. R. Kestner, S. A. Rice, and M. H. Cohen, J. Chem. Phys. **43**, 2614 (1965).
[22] J. Eloranta and V. A. Apkarian, J. Chem. Phys. **115**, 752 (2001).
[23] H.-J. Werner and P. J. Knowles, J. Chem. Phys. **89**, 5803 (1988).
[24] P. J. Knowles and H.-J. Werner, Chem. Phys. Lett. **145**, 514 (1988).
[25] D. E. Woon and T. H. Dunning, Jr., J. Chem. Phys. **100**, 2975 (1994).
[26] C. E. Moore, *Atomic Energy Levels* (National Bureau of Standards, Washington, DC, 1971).
[27] H. Herzberg, *Spectra of Diatomic Molecules*, 2nd ed. (Krieger, Melbourne, FL, 1989).
[28] H.-J. Werner and P. J. Knowles, J. Chem. Phys. **82**, 5053 (1985).
[29] P. J. Knowles and H.-J. Werner, Chem. Phys. Lett. **115**, 259 (1985).
[30] S. F. Boys and F. Bernardi, Mol. Phys. **19**, 553 (1970).
[31] M. R. A. Blomberg and P. E. M. Siegbahn, J. Chem. Phys. **78**, 5682 (1983).
[32] S. R. Langhoff and E. R. Davidson, Int. J. Quantum Chem. **8**, 61 (1974).
[33] MOLPRO is a package of *ab initio* programs written by H.-J. Werner and P. J. Knowles, with contributions from R. D. Amos, A. Bernhardsson, A. Berning, P. Celani, D. L. Cooper, M. J. O. Deegan, A. J. Dobbyn, F. Eckert, C. Hampel, G. Hetzer, T. Korona, R. Lindh, A. W. Lloyd, S. J. McNicholas, F. R. Manby, W. Meyer, M. E. Mura, A. Nicklass, P. Palmieri, R. Pitzer, G. Rauhut, M. Schütz, H. Stoll, R. Tarroni, and M. Thorsteinsson.
[34] J. Dupont-Roc, Z. Phys. B: Condens. Matter **98**, 383 (1995).
[35] F. Ancilotto, F. Faccin, and F. Toigo, Phys. Rev. B **62**, 17035 (2000).
[36] A. R. Janzen and R. A. Aziz, J. Chem. Phys. **107**, 914 (1997).

[37] B. L. Hammond, W. A. Lester, Jr., and P. J. Reynolds, *Monte Carlo Methods in Ab Initio Quantum Chemistry* (World Scientific, River Edge, NJ, 1994).
[38] L. Lehtovaara, T. Kiljunen, and J. Eloranta, J. Comput. Phys. (to be published).
[39] M. D. Ray and G. P. Lafyatis, Phys. Rev. Lett. **76**, 2662 (1996).
[40] E. A. Pazyuk, V. I. Pupyshev, A. V. Stolyarov, and T. Kiyoshima, J. Chem. Phys. **116**, 6618 (2002).
[41] T. L. Kwok, S. Guberman, A. Dalgarno, and A. Posen, Phys. Rev. A **34**, 1962 (1986).
[42] S. L. Guberman and A. Dalgarno, Phys. Rev. A **45**, 2784 (1992).
[43] G. Staszewska and L. Wolniewicz, J. Mol. Spectrosc. **198**, 416 (1999).
[44] E. J. Heller, Acc. Chem. Res. **14**, 368 (1981).
[45] D. A. McQuarrie, *Statistical Mechanics* (University Science Books, Sausalito, CA, 2000).
[46] A. P. Hickman, W. Steets, and N. F. Lane, Phys. Rev. B **12**, 3705 (1975).
[47] P. W. Anderson, Phys. Rev. **86**, 809 (1952).
[48] S. Bloom and H. Margenau, Phys. Rev. **90**, 791 (1952).
[49] J. Eloranta and V. A. Apkarian (in preparation).
[50] H. Helm, D. P. de Bruijn, and J. Los, Phys. Rev. Lett. **53**, 1642 (1984).
[51] R. P. Freis and J. R. Hiskes, Phys. Rev. A **2**, 573 (1970).
[52] J. Reho, U. Merker, M. R. Radcliff, K. K. Lehmann, and G. Scoles, J. Chem. Phys. **112**, 8409 (2000).
[53] T. Yabuzaki in *Proceedings of 4th International Conference on Low Temperature Chemistry* (Jyväskylä, Finland, 2002).